Polarimetric Multi-View Stereo
Supplementary Material

Zhaopeng Cui[1]   Jinwei Gu[2]   Boxin Shi[3]   Ping Tan[1]   Jan Kautz[2]

[1]Simon Fraser University   [2]NVIDIA Research

[3]Artificial Intelligence Research Center, National Institute of AIST

The supplementary material contains the complete proof of the appendix in our paper and more experimental results as follows: Section 1 describes the detailed proof of Equations (1) and (2) as well as Proposition 1 in the main paper based on the Muller calculus [1]; Section 2 presents more quantitative evaluation on the synthetic data, the running time and more experiment on real data with the laser scanned ground truth.

1. Proof of Proposition 1

The polarization state of light can be represented by a 4×1 Stokes vector $\mathbf{S} = [S_0, S_1, S_2, S_3]^\top$ where S_0 describes the total intensity of the light, S_1 is the intensity difference between polarized components of electromagnetic wave parallel and perpendicular to the reference plane, S_2 indicates the intensity difference between polarized components in planes $45°$ and $-45°$ to the reference plane, and S_3 describes the circularly polarized radiation [1]. The effect of light-matter intersections (*e.g.*, reflection, transmission, polarizer) to the polarization state is represented with a 4×4 Muller matrix $\mathbf{M}$. When a beam passes through a polarizing element, its polarization state changes from $\mathbf{S}$ to $\mathbf{MS}$.
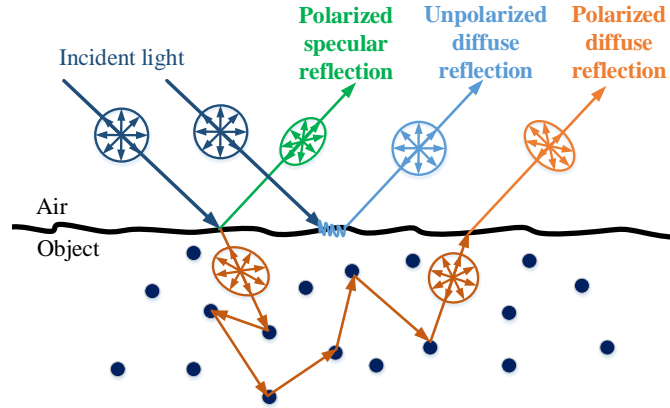

Figure 1: A diagram of surface reflection with mixed polarization. Reflected radiance for many surfaces includes three parts: **(1)** the polarized specular reflection (*i.e.*, highlight), **(2)** the polarized diffuse reflection (due to subsurface scattering and refraction), and **(3)** the unpolarized diffuse reflection (due to micro-facet rough surface reflection). The polarized specular reflection and the polarized diffuse reflection have a $\pi/2$ difference in phase angle. The circles with arrows show the polarization status: round circles – unpolarized, elliptic circles – partially polarized.

As shown in Figure 1, there are two polarized components in the reflected light. The polarized specular reflection is from the air-object surface, denoted by $\mathbf{S}_{sp}$. The polarized diffuse reflection is from the refraction from the depolarized subsurface scattered light to air, denoted by $\mathbf{S}_{dp}$. Both components will be measured by the camera via a linear polarizer. Let $\mathbf{S}_i$ be the Stokes vector for the illumination, $\mathbf{M}_{pol}(\theta)$ be the Muller matrix for the linear polarizer at angle θ, $\mathbf{M}_R$ and $\mathbf{M}_T$ denote the Muller matrices for Fresnel reflection and transmission, respectively. We have

$$\mathbf{S}_{sp} = \mathbf{M}_{pol}(\theta)\mathbf{M}_R\mathbf{S}_i, \qquad \mathbf{S}_{dp} = \mathbf{M}_{pol}(\theta)\mathbf{M}_T\mathbf{S}_d, \tag{1}$$
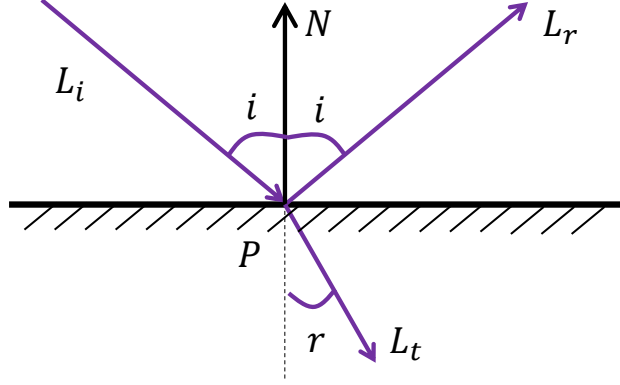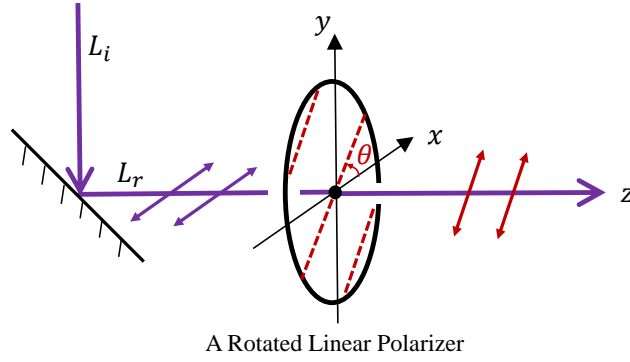
Figure 2: Reflection and transmission for polarized light.

A Rotated Linear Polarizer

Figure 3: The rotation angle θ of the polarizer in Equation (4) is defined as the angle between the polarization direction of the linear polarizer (*i.e.*, the red dash line) and the direction perpendicular to the plane of the incident illumination (*i.e.*, the x axis in this figure).

where $\mathbf{S}_d$ is the Stokes vector for the depolarized scattered light under surface.

For unpolarized illumination, $\mathbf{S}_i = L_i[1,0,0,0]$. $\mathbf{S}_d$ is also unpolarized due to random subsurface scattering, $\mathbf{S}_d = L_d[1,0,0,0]$. $\mathbf{M}_R$ and $\mathbf{M}_T$ are the Muller-Stokes matrices for Fresnel equations [1]. As shown in Figure 2, we have [1]

$$\mathbf{M}_R = f_R \begin{bmatrix} \cos^2\alpha_- + \cos^2\alpha_+ & \cos^2\alpha_- - \cos^2\alpha_+ & 0 & 0 \\ \cos^2\alpha_- - \cos^2\alpha_+ & \cos^2\alpha_- + \cos^2\alpha_+ & 0 & 0 \\ 0 & 0 & -2\cos\alpha_-\cos\alpha_+ & 0 \\ 0 & 0 & 0 & -2\cos\alpha_-\cos\alpha_+ \end{bmatrix}, \quad (2)$$

where $\alpha_\pm = i \pm r$ and $f_R = \frac{1}{2}\left(\frac{\tan\alpha_-}{\sin\alpha_+}\right)^2$, and

$$\mathbf{M}_T = f_T \begin{bmatrix} \cos^2\alpha_- + 1 & \cos^2\alpha_- - 1 & 0 & 0 \\ \cos^2\alpha_- - 1 & \cos^2\alpha_- + 1 & 0 & 0 \\ 0 & 0 & -2\cos\alpha_- & 0 \\ 0 & 0 & 0 & -2\cos\alpha_- \end{bmatrix}, \quad (3)$$

where $f_T = \frac{1}{2}\frac{\sin 2i \sin 2r}{(\sin\alpha_+ \cos\alpha_-)^2}$.

$\mathbf{M}_{pol}(\theta)$ is the Muller matrix for a rotated linear polarizer with angle θ. From [1], for an ideal rotated linear polarizer, we have

$$\mathbf{M}_{pol}(\theta) = \frac{1}{2}\begin{bmatrix} 1 & \cos 2\theta & \sin 2\theta & 0 \\ \cos 2\theta & \cos^2 2\theta & \sin 2\theta \cos 2\theta & 0 \\ \sin 2\theta & \sin 2\theta \cos 2\theta & \sin^2 2\theta & 0 \\ 0 & 0 & 0 & 0 \end{bmatrix}. \quad (4)$$

As shown in Figure 3, the angle θ is defined as the rotation angle between the polarization direction of the linear polarizer (*i.e.*, the red dash line) and the direction perpendicular to the plane of the incident illumination (*i.e.*, the x axis in Figure 3).
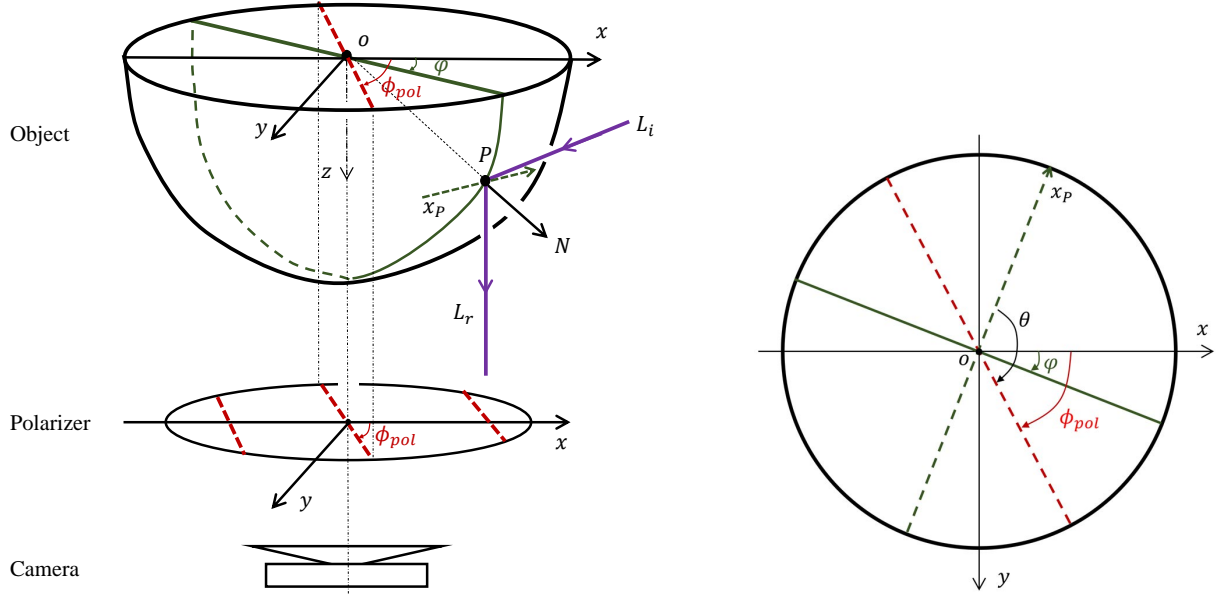

Figure 4: **Left**: A diagram of imaging a 3D object through a linear polarizer. The light reflected from a point P with surface normal N has two polarized reflection components, defined in Equation (9) and Equation (11) (*i.e.*, Equations (2) and (1) in the main paper), respectively. **Right**: Definitions of the three angles, φ, ϕ_{pol}, and θ, in the $x - y$ plane.

Consider imaging an object through a linear polarizer, as shown in Figure 4. For a point P on the object surface, suppose its surface normal is N. Let φ denote the azimuth angle of P, and ϕ_{pol} denote the angle between the polarization direction (*i.e.*, red dash line) of the polarizer and the x axis. Note that for the reflection and refraction at point P, the plane of the incident illumination is defined by surface normal N and the incident illumination L_i. The direction perpendicular to this plane is x_P. Thus, based on the definition in Figure 3, the rotation angle θ at point P is the angle between the polarization direction (*i.e.*, red dash line) and the direction x_P, and thus θ is given by

$$\theta = \phi_{pol} + \frac{\pi}{2} - \varphi. \tag{5}$$

The right side of Figure 4 shows a 2D view of the $x - y$ plane, with clear definitions of these three angles.

By the definition of the Stokes vector, the measured radiance for both polarized specular reflection and polarized diffuse reflection are the first element in the Stokes vectors,

$$I_{sp}(\phi_{pol}) = \mathbf{S}_{sp}(0), \qquad I_{dp}(\phi_{pol}) = \mathbf{S}_{dp}(0). \tag{6}$$

By putting Equation (2), Equation (3), Equation (4), and Equation (5) into Equation (1) and Equation (6), we can derive Equations (1) and (2) in the main paper. More specifically, we have

$$\mathbf{S}_{sp} = \mathbf{M}_{pol}(\theta)\mathbf{M}_R\mathbf{S}_i = \frac{1}{2}\begin{pmatrix} 1 & \cos 2\theta & \sin 2\theta & 0 \\ \cos 2\theta & \cos^2 2\theta & \sin 2\theta \cos 2\theta & 0 \\ \sin 2\theta & \sin 2\theta \cos 2\theta & \sin^2 2\theta & 0 \\ 0 & 0 & 0 & 0 \end{pmatrix} \frac{L_i}{2}\left(\frac{\tan \alpha_-}{\sin \alpha_+}\right)^2 \begin{pmatrix} \cos^2 \alpha_- + \cos^2 \alpha_+ \\ \cos^2 \alpha_- - \cos^2 \alpha_+ \\ 0 \\ 0 \end{pmatrix} \tag{7}$$

and

$$\mathbf{S}_{dp} = \mathbf{M}_{pol}(\theta)\mathbf{M}_T\mathbf{S}_d = \frac{1}{2}\begin{pmatrix} 1 & \cos 2\theta & \sin 2\theta & 0 \\ \cos 2\theta & \cos^2 2\theta & \sin 2\theta \cos 2\theta & 0 \\ \sin 2\theta & \sin 2\theta \cos 2\theta & \sin^2 2\theta & 0 \\ 0 & 0 & 0 & 0 \end{pmatrix} \frac{L_d}{2}\frac{\sin 2i \sin 2r}{(\sin \alpha_+ \cos \alpha_-)^2} \begin{pmatrix} \cos^2 \alpha_- + 1 \\ \cos^2 \alpha_- - 1 \\ 0 \\ 0 \end{pmatrix} \tag{8}$$

From Equation (5), we have $\theta = \phi_{pol} + \frac{\pi}{2} - \varphi$. Thus, we have

$$
\begin{aligned}
I_{sp}(\phi_{pol}) = \mathbf{S}_{sp}(0) &= \frac{L_i}{4}\left(\frac{\tan\alpha_-}{\sin\alpha_+}\right)^2\left(\left(\cos^2\alpha_- + \cos^2\alpha_+\right) + \left(\cos^2\alpha_- - \cos^2\alpha_+\right)\cos 2\theta\right) \\
&= \frac{I_{max}^{sp} + I_{min}^{sp}}{2} + \frac{I_{max}^{sp} - I_{min}^{sp}}{2}\cos(2\theta) \\
&= \frac{I_{max}^{sp} + I_{min}^{sp}}{2} + \frac{I_{max}^{sp} - I_{min}^{sp}}{2}\cos(2(\phi_{pol} - \varphi + \frac{\pi}{2})),
\end{aligned} \tag{9}
$$

where

$$
I_{max}^{sp} = \frac{L_i}{2}\left(\frac{\tan\alpha_-}{\sin\alpha_+}\right)^2\cos^2\alpha_-, \qquad I_{min}^{sp} = \frac{L_i}{2}\left(\frac{\tan\alpha_-}{\sin\alpha_+}\right)^2\cos^2\alpha_+. \tag{10}
$$

Similarly, we have

$$
\begin{aligned}
I_{dp}(\phi_{pol}) = \mathbf{S}_{dp}(0) &= \frac{L_d}{4}\frac{\sin 2i \sin 2r}{(\sin\alpha_+\cos\alpha_-)^2}\left(\left(\cos^2\alpha_- + 1\right) + \left(\cos^2\alpha_- - 1\right)\cos 2\theta\right) \\
&= \frac{I_{max}^{dp} + I_{min}^{dp}}{2} + \frac{I_{max}^{dp} - I_{min}^{sp}}{2}\cos(2(\theta - \pi/2)) \\
&= \frac{I_{max}^{dp} + I_{min}^{dp}}{2} + \frac{I_{max}^{dp} - I_{min}^{dp}}{2}\cos(2(\phi_{pol} - \varphi)),
\end{aligned} \tag{11}
$$

where

$$
I_{max}^{dp} = \frac{L_d}{2}\frac{\sin 2i \sin 2r}{(\sin\alpha_+\cos\alpha_-)^2}, \qquad I_{min}^{dp} = \frac{L_d}{2}\frac{\sin 2i \sin 2r}{(\sin\alpha_+\cos\alpha_-)^2}\cos^2\alpha_-. \tag{12}
$$

Note that Equation (9) and Equation (11) are exactly Equation (2) and Equation (1) in the main paper. Many real-world objects have both the polarized specular reflection and the polarized diffuse reflection, as well as an unpolarized diffuse reflection. So we have

$$
I(\phi_{pol}) = I_d + I_{dp}(\phi_{pol}) + I_{sp}(\phi_{pol}), \tag{13}
$$

where I_d is the unpolarized diffuse reflection that does not vary with the polarization angle ϕ_{pol}. By inserting Equation (9) and Equation (11) in Equation (13) and considering $\cos(x \pm \pi) = -\cos(x)$, we have

$$
\begin{aligned}
I(\phi_{pol}) &= I_d + \frac{I_{max}^{dp} + I_{min}^{dp}}{2} + \frac{I_{max}^{dp} - I_{min}^{dp}}{2}\cos(2(\phi_{pol} - \varphi)) + \frac{I_{max}^{sp} + I_{min}^{sp}}{2} + \frac{I_{max}^{sp} - I_{min}^{sp}}{2}\cos(2(\phi_{pol} - \varphi + \frac{\pi}{2})), \\
&= \frac{I_{max} + I_{min}}{2} + \frac{I_{max} - I_{min}}{2}\cos(2(\phi_{pol} - \phi)),
\end{aligned} \tag{14}
$$

where ϕ is defined as the phase angle, I_{max} and I_{min} are the maximum and minimum observed intensities. When polarized diffuse reflection dominates ($\frac{I_{max}^{dp} - I_{min}^{dp}}{2} > \frac{I_{max}^{sp} - I_{min}^{sp}}{2}$), we have

$$
\phi = \varphi, \quad I_{max} = I_d + I_{max}^{dp} + I_{min}^{sp}, \quad I_{min} = I_d + I_{min}^{dp} + I_{max}^{sp}. \tag{15}
$$

When polarized specular reflection dominates ($\frac{I_{max}^{sp} - I_{min}^{sp}}{2} > \frac{I_{max}^{dp} - I_{min}^{dp}}{2}$), we have

$$
\phi = \varphi - \frac{\pi}{2}, \quad I_{max} = I_d + I_{max}^{sp} + I_{min}^{dp}, \quad I_{min} = I_d + I_{min}^{sp} + I_{max}^{dp}. \tag{16}
$$

From Equations (14), (15) and (16), we have Proposition 1 in the main paper.

Structure-from-Motion:	23
Phase Angle Estimation:	25
Initialization (Depth Estimation):	352
(*)Resolving $\pi/2$-Ambiguity:	1096
(*)Depth Propagation:	132
(*)Depth Optimization:	1475
Depth Fusion:	215
Total:	3318

Table 1: Running time (in seconds) on VASE. Note that the steps with (*) are not optimized as we currently computed them sequentially for each view. They can be easily parallelized.
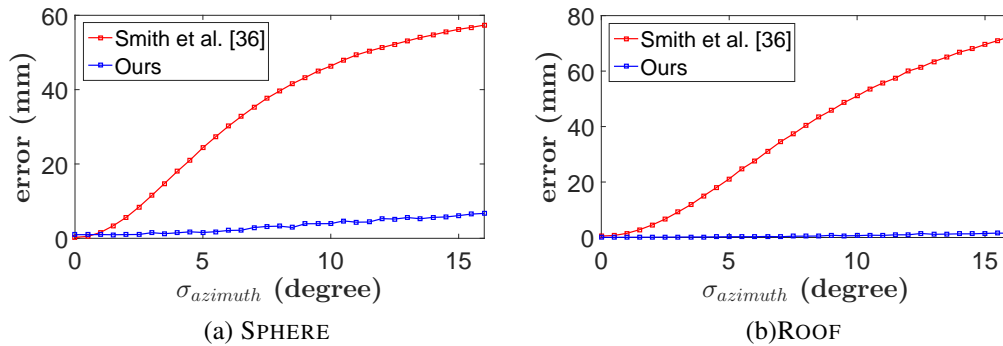

(a) SPHERE (b)ROOF

Figure 5: Average reconstruction errors of the synthetic examples with varying noise in the azimuth angle.

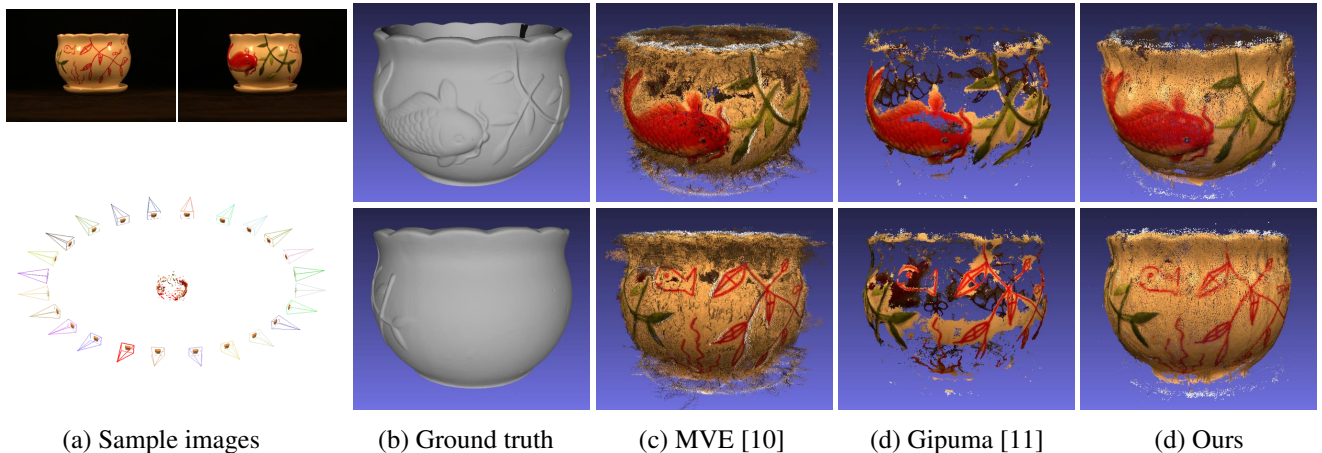(a) Sample images (b) Ground truth (c) MVE [10] (d) Gipuma [11] (d) Ours

Figure 6: Comparison with state-of-the-art MVS methods [10, 11] for complete reconstruction.

2. More experimental results

We conducted the quantitative evaluation against noises on the synthetic data SPHERE and ROOF. As our method maintains only one common parameter the azimuth angle with [36], for fair comparison, we set all other parameters to be the ground truth and add a Gaussian noise to the azimuth angle map with varying $\sigma_{azimuth}$ from 0 to 16 degrees with a step of 0.5 degree. The mean error is used for comparison. As it is shown in Figure 5, our method shows more stable performance under various noises than [36].

Figure 6 shows the comparison of our method and two state-of-the-art MVS methods [10, 11] on a real dataset with the laser scanned ground truth. As there are obvious specular highlights and featureless parts on the body of the flowerpot, Gipuma [11] fail to reconstruct large parts of the flowerpot. The result of MVE [10] is noisy and it also has larges holes in some featureless parts (e.g. the parts above the red fish). In contrast, our method generates more complete and smooth model.

We tested the running time of our method for one of our dataset (VASE) on a desktop PC (two 2.3GHz Intel Xeon E5-2650 CPUs and one Nvidia Quadro K5200 GPU). The result is listed in Table 1.

References

[1] E. Collett. *Field Guide to Polarization*. SPIE, 2005. 1, 2